Preprint
Allende G., D'Amico S., Montenbruck O., Hugentobler U., Delpech M.;
Radio-frequency sensor fusion for relative navigation of formation flying satellites;
International Journal of Space Science and Engineering (2015).

Radio-frequency sensor fusion for relative navigation of formation flying satellites

Abstract: The increasing need for robustness, reliability and flexibility of relative navigation systems imposed by the current and future autonomous formation flying missions, calls for the implementation of solutions using an alternative approach to single-sensor systems. These schemes possess different levels of availability, mainly driven by sensor failure and mission orbit profiles. The data obtained from the Global Positioning System (GPS) and Formation Flying Radio-Frequency (FFRF) sensors from the nominal phase of the PRISMA mission provide an opportunity for the implementation of an extended approach for the generation of relative navigation solutions. The present study introduces the design of a simple relative navigation filter based on the sensor fusion concept, which makes use of differential GPS and FFRF measurements obtained from the on-board sensors. The filter design uses the Hill-Clohessy-Wiltshire and Yamanaka-Ankersen relative dynamics models as well as numerical integration methods including the J2-perturbation for the state and associated covariance matrix propagation. The design is tested using flight data obtained during representative formation flying operations of the PRISMA mission.

Keywords: Formation Flying Radio-Frequency; Global Positioning System; Relative Navigation; Sensor Fusion; Prima

1 Introduction

The use of the GPS for relative navigation of formation flying satellites in Low Earth Orbit (LEO) has achieved a high degree of maturity over the past 15 years, mainly due to the capability of this navigation system of providing the required accuracy and precision for various formation flying profiles, such as rendezvous and baseline determination (D'Errico, 2013). Notable examples include the ATV-ISS rendezvous operations and the GRACE and TanDEM-X baseline determination missions (Jäggi, et.al., 2007; Montenbruck, et.al., 2011; Pinard, et.al., 2007).

The recent PRISMA mission represents a milestone in the field of formation flying given that it provides an in-orbit test-bed for new sensor and actuators systems. Among these systems, the FFRF sensor represents the first non-GPS RF-based metrology instrument for relative navigation to be flown in an actual mission (Grelier, et.al., 2010). The main concept behind the FFRF sensor is to provide a precise relative navigation solution independent of any Global Navigation Satellite System (GNSS) through the generation of its own navigation signals. It is thus capable of being used not only in LEO missions, but also in Highly Elliptical Orbits (HEO) (Delpech, et.al., 2009). The FFRF sensor was successfully commissioned and tested during the PRISMA nominal mission period and was capable of providing precise relative navigation solutions for the execution of Guidance, Navigation and Control (GNC) activities (Grelier, et.al., 2010).

Copyright © 2009 Inderscience Enterprises Ltd.

Until recent years, the use of GPS has been considered as the sole primary technology to obtain relative navigation solutions in formation flying missions. However, the increasing need for robustness, reliability and flexibility of such solutions calls for the implementation of designs using an extended approach to single-sensor or isolated-sensor systems, which are always prone to failure and might possess different levels of availability. In particular, the HEO scenario represents a tough environment for GPS-only relative navigation systems (Ardaens, et.al., 2013), demanding the usage of a different approach and/or instrumentation if a precision at sub-meter levels needs to be preserved. The FFRF technology represents a suitable single-sensor solution for such cases, but this would imply that good and reliable GPS measurements might be misspent for those orbit phases where they are available.

The GPS and FFRF data obtained from the PRISMA mission provides the opportunity of implementation of alternative approaches to single-sensor relative navigation systems. The present study introduces the design of a simple extended Kalman filter (EKF) for relative navigation, considering the sensor fusion concept and making use of differential GPS and FFRF measurements in order to increase the robustness, reliability and availability of the delivered solution.

2 RF measurements and sensor fusion architecture

2.1 FFRF measurements

The FFRF sensor has been derived from the GPS technology and it is capable of producing, for each spacecraft in the formation, relative distance and line of sight (LOS) measurements concerning all its companions. The distance between two satellites is obtained by combining their respective pseudorange measurements in order to remove inter-equipment clock bias and for this purpose navigation data must be exchanged through the inter-satellite link (ISL) provided by the FFRF instrument (Delpech, et.al., 2009). The LOS measurements rely on interferometry techniques and they are obtained by measuring the carrier phase difference between two antennas (master and slave) on the triplet antenna base of the FFRF subsystem (Grelier, et.al., 2010), as depicted in Figure 1.

When distance and LOS measurements make use of carrier phase in order to achieve the nominal precision, it is necessary to execute additional procedures and algorithms for Integer Ambiguity Resolution (IAR). Such procedures are executed first to solve ambiguity in LOS measurements in order to be able to solve ambiguity on distance. This approach mitigates multipath effects which are direction dependent (Delpech, et.al., 2009).

2.2 GPS measurements

As a result from the diverse system requirements of recent formation flying missions, the GPS technology has been used for the generation of different kind of products for off-line and real-time processing. Current approaches for the generation of these products are based on filtering using dynamical models (D'Amico, et.al., 2009), which make them unsuitable for blending with pure kinematic FFRF measurements. Instead, based on the targeted accuracy at the centimetre-level and driven by the mechanical characteristics of FFRF measurements, a single dynamical filtering approach that makes use of purely kinematic GPS measurements is desirable. For this purpose, the GPS navigation fixes obtained from code measurements are too coarse to be considered and hence a set of more precise measurements is preferred.

Figure 1 PRISMA spacecraft. Mango (left) and Tango (right). (Source: SSC)

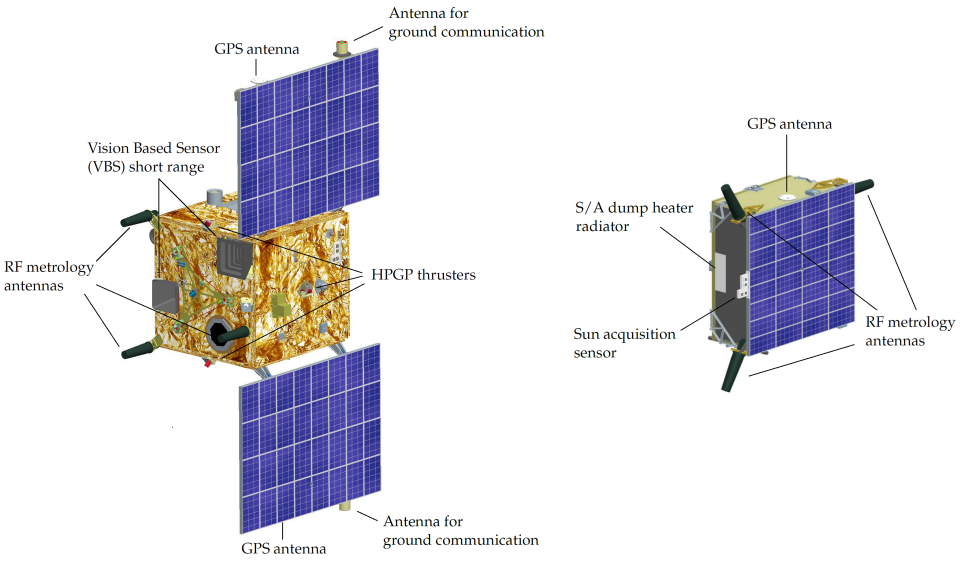

As an add-on solution to the Precise Orbit Determination (POD) product obtained from the DLR's GPS High precision Orbit determination Software Tools (GHOST), a purely kinematic relative position solution can be computed from the ambiguity-fixed differential carrier phases (Ardaens, et.al., 2012; D'Amico, et.al., 2012). Thus, this product is not available for real-time processing but has been provided from off-line processing in order to be used for the present study. However, research on Precise Point Positioning (PPP) for LEO satellites might provide in the near future a similar precision to those obtained off-line by means of differential GPS techniques (Hauschild and Montenbruck, 2008).

2.3 Sensor fusion architecture

The sensor fusion concept has been considered and successfully applied for several years for terrestrial applications (both military and civilian) where features such as robustness and flexibility are key drivers. Although not a new concept, the emergence of new sensors, advanced processing techniques and improved processing hardware make data fusion increasingly appealing (Hall and Llinas, 1997). This argument can be extended to the case of sensor fusion for relative navigation of formation flying satellites.

Broadening common terminology, the sensor fusion scheme proposed in the present study uses the term *track* fusion for the merging of estimates from individual sensor tracks whereas the term *scan* fusion is used for algorithms that combine observations from different sensors (Durrant-Whyte, H., 2001). The reader is referred to Liggins, et.al. (2008) for a thorough revision of techniques and standard-level terminologies. In the context of the proposed design, the FFRF data track provides measurements which are suitable for scan fusion, namely at the data level. On the other hand, the GPS data track results in an estimated state which is adequate for track fusion at the state vector level. Provided the characteristics of the available data from both sensors and the targeted solution (dynamically-filtered with centimeter-level accuracy), it is not possible to constrain the design of the algorithm to a single type of fusion level. Therefore, the proposed architecture combines these two sources

Figure 2 FFRF and GPS sensor fusion architecture

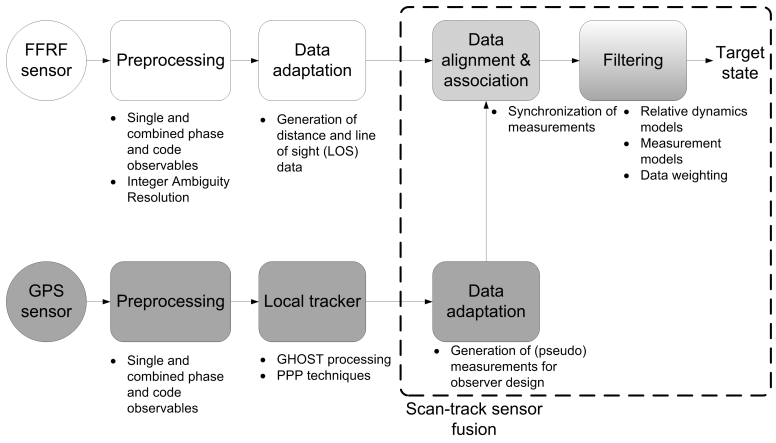

of information in a hybrid scan-track (data-state vector) fusion algorithm, as sketched in Figure 2, using GPS data as pseudo-measurements so as to be included into the scheme at the same level of FFRF data. The box in dashed line indicates the part of the architecture that was implemented in the present study.

3 Filter design

The main objective of the present filter design is the delivery of relative navigation solutions of the deputy (Mango in the PRISMA context) spacecraft's center of mass with the best achievable precision (centimetre-level) in the local orbital frame by making use of FFRF and GPS measurements. The local orbital coordinate frame (also known as Euler-Hill frame and denoted as $\mathcal{H}$) is referred to the target (Tango in the PRISMA context) spacecraft's center of mass and constructed out of the radial, tangential (along-track) and normal (cross-track) unit vectors of the target absolute orbit in a given reference frame. In order to achieve a centimetre-level precision, the filter has to cope with biases of the FFRF data, which may affect significantly the final relative navigation solution if they are not considered. To this end, the estimated data contained in the filter state vector $\mathbf{y}$, must include the relative dynamics state vector (position and velocity) as well as the FFRF float biases.

3.1 Observation and measurement models

3.1.1 GPS sensor

The precise kinematic GPS products are provided by GHOST in an Earth-Centered Earth-Fixed (ECEF) reference frame (denoted as $\mathcal{E}$) in the form of absolute position vectors for each spacecraft in the formation (given as $\mathbf{r}_{\text{M}}^{\mathcal{E}}$ for Mango and as $\mathbf{r}_{\text{T}}^{\mathcal{E}}$ for Tango). Thereby, the GPS observation model can be expressed as

$$\mathbf{z}^g = \begin{bmatrix} \Delta x^{\mathcal{H}} \\ \Delta y^{\mathcal{H}} \\ \Delta z^{\mathcal{H}} \end{bmatrix} = \boldsymbol{R}_{\mathcal{E}}^{\mathcal{H}}(\mathbf{x}_r) \cdot [\mathbf{r}_{\text{M}}^{\mathcal{E}} - \mathbf{r}_{\text{T}}^{\mathcal{E}}] + \boldsymbol{\epsilon}_G \tag{1}$$

Figure 3 Errors in GPS pseudo-measurements in the Euler-Hill frame from 2010/10/28-16:00 to 2010/10/28-18:00 UTC, using POD as reference. During this data arc, the two spacecraft perform various formation flying operations.

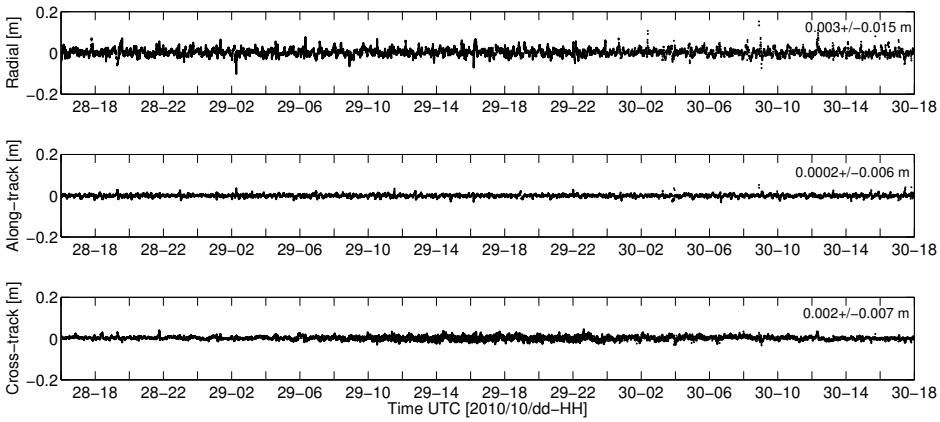

Here, the rotation matrix $\boldsymbol{R}_{\mathcal{E}}^{\mathcal{H}}$ has an explicit dependence to a reference orbit $\mathbf{x}_r$ which is used to define the frame and can be generated from the highly-available GPS navigation fixes of the Tango spacecraft. The GPS observation vector $\mathbf{z}^g$ denotes the relative position of the Mango spacecraft's center of mass in the $\mathcal{H}$ frame and is used as a set of pseudo-measurements in the filter algorithm. The vector $\boldsymbol{\epsilon}_G$ represents noise and other unmodelled factors in the GPS observables.

In order to include this GPS data set in the fusion filter, it must be assessed so that their statistical properties can be properly reflected in the filtering algorithm. A comparison between precise dynamic (from precise orbit determination or POD) and kinematic products provides an indication of the expected errors, as shown in Figure 3 for a data arc of 50 hours. The POD products used in the present study have a typical relative navigation precision of better than 1 mm (1D rms) (Kroes, R., 2006). As depicted in Figure 3, the kinematic GPS solution exhibits an rms error of around 6 mm and 7 mm in the along-track and cross-track components, respectively, whereas the radial component shows an rms error of around 1.5 cm. The slightly worse noise levels in the radial component are a consequence of the bad local vertical geometry of the formation with respect to the GPS constellation.

The form of the vector given by equation (1) can be used to define the GPS measurement model (namely, modelled observations) to be used in the filter algorithm. If $\hat{\mathbf{y}}$ denotes the estimated filter state vector in the filtering algorithm, it can be used to linearise the GPS measurement model, which explicitly can be expressed as

$$h^g = h^g(\Delta x^{\mathcal{H}}(\hat{\mathbf{y}}), \Delta y^{\mathcal{H}}(\hat{\mathbf{y}}), \Delta z^{\mathcal{H}}(\hat{\mathbf{y}}), \mathbf{x}_r) \tag{2}$$

where the dependence on the reference orbit $\mathbf{x}_r$ is used for the construction of the $\mathcal{H}$ frame.

3.1.2 FFRF sensor

Once the IAR procedures are executed, the FFRF sensor is designed to deliver measurements denoting the relative position of the phase center of the Tango active antenna expressed in

Figure 4 Errors in FFRF measurements in the RF frame from 2010/10/28-16:00 to 2010/10/28-18:00 UTC, using POD as reference. During this data arc, the two spacecraft perform various formation flying operations

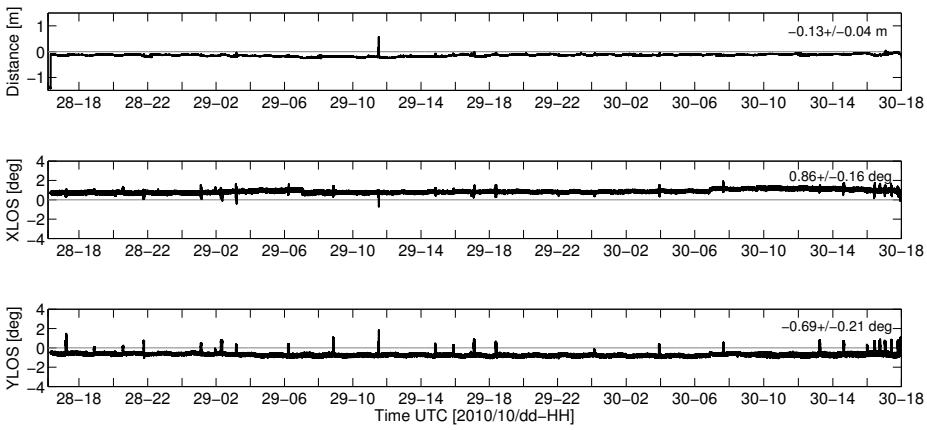

the RF frame (denoted as $\mathcal{F}$), given by the coordinates $\Delta x^{\mathcal{F}}$, $\Delta y^{\mathcal{F}}$ and $\Delta z^{\mathcal{F}}$. The $\mathcal{F}$ frame is referred to the phase center of the master Rx/Tx antenna on the Mango spacecraft and axes defined to match the body-fixed frame of the Mango spacecraft (Delpech, et.al., 2009) (see Figure 1). The FFRF observation model can be constructed from the computation of the relative distance d and the LOS measurements in the x and y components (x_{LOS} and y_{LOS}, respectively), as follows

$$\mathbf{z}^f = \begin{bmatrix} d \\ x_{LOS} \\ y_{LOS} \end{bmatrix} = \begin{bmatrix} \sqrt{(\Delta x^{\mathcal{F}})^2 + (\Delta y^{\mathcal{F}})^2 + (\Delta z^{\mathcal{F}})^2} \\ \Delta x^{\mathcal{F}}/d \\ \Delta y^{\mathcal{F}}/d \end{bmatrix} + \mathbf{b} + \boldsymbol{\epsilon}_F \tag{3}$$

where $\mathbf{z}^f$ is a vector of FFRF measurements. The vector $\mathbf{b}$ represents the cumulated bias affecting the distance and LOS measurements due to residual electrical biases along RF cables, uncertainty on the location of Rx antennas phase center and residual multipath errors (Delpech, et.al., 2009). The vector $\boldsymbol{\epsilon}_F$ represents noise and other unmodelled factors in the FFRF observables.

As in the case of the GPS data set, in order to include FFRF data in the filtering algorithm, it must be first assessed in order to analyse their statistical properties. Figure 4 shows the errors in FFRF measurements expressed in the $\mathcal{F}$ frame as defined by equation (3). The errors are assessed for a data arc of 50 hours using POD products as reference.

From the analysis of the FFRF data assessment shown in Figure 4, it is possible to observe the non-constant bias in LOS measurements, whose fluctuations are attributed to sensor temperature variations, as shown by Delpech, et.al. (2011) . In addition, large angular excursions in LOS measurements are present due to multipath effects during attitude manoeuvres (Guidotti, et.al., 2011).

According to the proposed filter design, the estimated filter state vector and the FFRF measurements are expressed in different coordinate frames, which implies that the FFRF measurement model must depend on the attitude quaternions of the Tango and Mango

spacecraft ($\mathbf{q}_{\text{T}}$ and $\mathbf{q}_{\text{M}}$, respectively) as well as on the reference orbit $\mathbf{x}_r$ for the construction of the $\mathcal{H}$ frame. In addition, the evaluation of the measurement model in the navigation filter makes it dependent on the estimated vector $\hat{\mathbf{y}}$. Furthermore, according to the FFRF sensor design, the distance and LOS measurements are not available at exactly the same times (Delpech, et.al., 2009), which indicates that two different models should be considered for the filtering algorithm, as follows

$$h^d = h^d(d(\hat{\mathbf{y}}), \mathbf{q}_{\text{M}}, \mathbf{q}_{\text{T}}, \mathbf{x}_r) \tag{4a}$$

$$h^l = h^l(x_{LOS}(\hat{\mathbf{y}}), y_{LOS}(\hat{\mathbf{y}}), \mathbf{q}_{\text{M}}, \mathbf{q}_{\text{T}}, \mathbf{x}_r) \tag{4b}$$

where the dependence of the model on the estimated filter state vector might not be in general the same for both type of measurements.

3.2 Relative dynamics

The filtering algorithm requires the prediction of the state (and its associated error covariance matrix) which in turn is used as a-priori information in the computation of the updated state. This prediction step is aided from the knowledge of the dynamics of the spacecraft in the formation. Two well-known linear analytical relative dynamics models for unperturbed motion are used in the present design. One of them can be applied for relative motion with circular target orbits and it is derived from the works of Clohessy and Wiltshire (1960) and Hill (1878) and therefore denoted henceforth as the Hill-Clohessy-Wiltshire (HCW) model. The interested reader is referred to Alfriend, et.al. (2010) for a recent treatment of this solution. The second model under consideration is the so-called Yamanaka-Ankersen (YA) model, which can be applied to problems with elliptical target orbits of arbitrary eccentricity (Yamanaka and Ankersen, 2002). These models are particularly appealing given their simplicity, but they provide only approximations for the case of perturbed motion. In particular, the zonal geopotential coefficient J2 causes one of the largest perturbations for LEO satellites and should be considered in the description of the relative motion of the spacecraft in the formation, given the targeted precision.

Table 1 Relative dynamics strategies for state propagation

State vector propagation	**State covariance matrix propagation**
Analytical model (Hill-Clohessy-Wiltshire & Yamanaka-Ankersen)	
Difference of absolute states from numerical integration	Analytical model (Hill-Clohessy-Wiltshire & Yamanaka-Ankersen)

A more precise evaluation of the relative dynamics calls for the analysis of orbital perturbations but in order to keep the design as simple as possible (yet accurate) only the J2-perturbation is considered. However, due to the complexity of the analytical equations

of perturbed motion, there are no simple implementations[1] of a linearised model and the dynamical equations must be integrated numerically.

On the other hand, the state error propagation in the filtering algorithm still requires the usage of a linear relative dynamics model. Even though the HCW and YA models are sub-optimal models, their relative simplicity and the provided good approximations for the description of relative motion make them suitable for propagation of the associated state covariance matrix. Table 1 shows a summary of the different approaches for the relative dynamics of the spacecraft formation flying implemented in the present study.

3.3 Algorithm description

Given that both the relative dynamics and measurements models under consideration are non-linear, the proposed fusion algorithm is based on an EKF, for which a set of linearised models should be properly defined. Section 3.2 has already introduced the linearised relative dynamics models to be used and the inclusion of linearised versions of the measurement models given by equations (2) and (4) into the EKF should be considered as part of the algorithm description.

3.3.1 Bias estimation

According to the model given by equation (3), the FFRF observables are subject to biases that may degrade a relative navigation solution if not coped for. The biases in XLOS and YLOS measurements can be effectively tackled by estimation and previous analyses of the on-board FFRF-based relative navigation filter have demonstrated the feasibility of this approach (Delpech, et.al., 2011; Guidotti, et.al., 2011).

In order to understand how to manage the biases of the FFRF measurements in the filter design, assume for the moment that a set of LOS and distance measurements are available at the same time t_m. Dropping the explicit notation of coordinate frames for simplicity and denoting the relative dynamics state vector (comprising relative position and velocity) as $\Delta\mathbf{x} = [\Delta\mathbf{r}, \Delta\dot{\mathbf{r}}]^T$, the general observation model of equation (3) can be fully written as

$$\mathbf{z}^f(t_m) = \boldsymbol{H}^f(t_m)\Delta\mathbf{x}(t_m) + \mathbf{B}^f(t_m)\mathbf{b}(t_m) + \boldsymbol{\epsilon}_F(t_m) \tag{5}$$

where $\boldsymbol{H}^f$ is the linearised version of models shown in equation (4) and f may take the values d or l (distance and LOS, respectively). The matrix $\mathbf{B}^f$ maps the bias vector $\mathbf{b}$ into the FFRF measurement vector $\mathbf{z}^f$. Similarly, the bias vector can be propagated in time using a general Gauss-Markov model, as follows

$$\mathbf{b}(t_k) = \mathbf{G}(t_k, t_{k-1})\mathbf{b}(t_{k-1}) + \mathbf{w}_b(t_k) \tag{6}$$

The measurement noise vector $\boldsymbol{\epsilon}_F$ and the bias process noise vector $\mathbf{w}_b$ are assumed as Gaussian, zero mean and temporally uncorrelated, with covariance matrices $\mathbf{R}^f$ and $\mathbf{Q}_b$, respectively.

Existing approaches such as the Gim-Alfriend (Gim and Alfriend, 2003) and Montenbruck-D'Amico (D'Amico and Montenbruck, 2006; Montenbruck, et.al., 2006) analytical models require transformations of relative orbital elements, making them unsuitable for the present design, for which low complexity is one of the driving factors

The state transition matrix (STM) of a given analytical relative dynamics model $\boldsymbol{\Phi}$ can be augmented into matrix $\mathbf{\Phi}$ by considering the bias propagation matrix $\mathbf{G}$ from equation (6), as follows

$$\mathbf{\Phi} = \begin{bmatrix} \boldsymbol{\Phi}_{6\text{x}6} & \mathbf{0}_{6\text{x}3} \\ \mathbf{0}_{3\text{x}6} & \mathbf{G}_{3\text{x}3} \end{bmatrix} \tag{7}$$

with an associated augmented process noise covariance matrix $\mathbf{Q}$ in the EKF algorithm. This augmented STM is suitable for state error propagation during the time update of the filtering scheme.

Expressing the filter state vector as $\mathbf{y} = [\Delta\mathbf{x}, \mathbf{b}]^T$, the Gauss-Markov and the general (FFRF) measurement models of the system are given respectively by

$$\mathbf{y}(t_k) = \mathbf{\Phi}(t_k, t_{k-1})\mathbf{y}(t_{k-1}) + \mathbf{u}(t_k) + \mathbf{w}(t_k) \tag{8a}$$

$$\mathbf{z}^f(t_m) = \mathbf{H}^f(t_m)\mathbf{y}(t_m) + \boldsymbol{\epsilon}_F(t_m) \tag{8b}$$

where the augmented linearised measurement model is given by $\mathbf{H}^f = [\boldsymbol{H}^f \mathbf{B}^f]$ and $\mathbf{u}$ represents a control input to the system, such as a manoeuvre burn. Equation (8a) represents the linear system model that is suitable to provide an a-priori state vector estimate before the innovation of the EKF and takes into account FFRF bias propagation. It can be used as long as the errors introduced by the linearised relative dynamics can be tolerated. The same approach for the expression of a general linearised measurement model can easily be extended for the case of GPS measurements, using $\mathbf{H}^g = [\boldsymbol{H}^g \mathbf{0}_{3\text{x}3}]$ in equation (8b), where $\boldsymbol{H}^g$ is the linearised version of the model given by equation (2).

Furthermore, according to equation (5) and considering independent sets of FFRF distance, FFRF LOS and GPS measurements, their statistical properties can be encoded into the noise covariance for every measurement equation, expressed in the matrices $\mathbf{R}^d$, $\mathbf{R}^l$ and $\mathbf{R}^g$, respectively.

3.3.2 Synchronization of measurements and filtering algorithm

One of the main problems that sensor fusion systems face is the non-synchronicity of measurements. This is a natural consequence derived from sensor design and the different sample rates and latencies. However, this situation is not limited to the use of diverse sensors but it can be present even in single-sensor designs. An example of this is the FFRF instrument, which provides LOS and distance measurements approximately every second but at different times and thus, a synchronization strategy should be considered if the measurements are to be used in a sequential estimation algorithm (Delpech, et.al., 2009). In addition, when GPS measurements (provided every 10 or 20 seconds for the present study) are incorporated into the filter design, this synchronization strategy must be extended in order to properly manage the timing characteristics of such measurements.

Considering the a-synchronicity among LOS and GPS measurements and the non-sequent delivery rate of distance measurements, the present design is focused on the maximal usage of available FFRF measurements generating a relative navigation solution by executing a filter innovation step when a distance or a set of LOS measurements are available. Based on the primary design of the on-board relative navigation filter described by Delpech, et.al. (2009), the delivery rate of the solution can be matched to the LOS

measurements latency, but an equivalent approach can easily be obtained by matching the delivery rate to the distance measurement times.

The present design has the capability of performing a state propagation by using solely (linearised) analytical models or by means of a hybrid approach where a numerical integration method for state vector propagation is included in the algorithm, as shown in Table 1. As expected, performing a numerical integration (considering the inclusion of J2-perturbation) provides more precision but also imposes a higher computational burden. On the other hand, the effective mitigation of some errors caused by the presence of biases in LOS measurements highly relies in the precision of the relative dynamics model. Thus, the selection of the proper approach for state propagation is based on a trade-off between the required precision for a given mission phase and computational burden. State vector propagation using only an analytical model can be performed by using equation (8a), whereas a hybrid approach requires some extra procedures. The results presented in section 4 were obtained by using the latter, which is hereafter developed.

Having a filter state vector estimate (along with a set of absolute state vectors for both spacecraft) at time t_0 a solution can be computed at the execution time t_e if either a set of FFRF LOS or GPS measurements is available. The predicted state is obtained first by performing a numerical integration of the estimate at time t_0 of the absolute dynamics state vectors of the Tango and Mango spacecraft (denoted as $\hat{\mathbf{x}}_{\mathrm{T}}$ and $\hat{\mathbf{x}}_{\mathrm{M}}$, respectively), as follows

$$\hat{\mathbf{x}}_{\mathrm{T}}^{\mathcal{I}-}(t_e) = f(t_e, t_0; \hat{\mathbf{x}}_{\mathrm{T}}^{\mathcal{I}}(t_0)) \tag{9a}$$

$$\hat{\mathbf{x}}_{\mathrm{M}}^{\mathcal{I}-}(t_e) = f(t_e, t_0; \hat{\mathbf{x}}_{\mathrm{M}}^{\mathcal{I}}(t_0)) \tag{9b}$$

where the function $f(\cdot)$ represents a numerical integrator using the Runge-Kutta 4 method for the two-body problem considering a J2-perturbed motion. The notation $\mathcal{I}$ denotes a vector referred to an Earth-Centered Inertial (ECI) reference frame.

The obtained absolute orbit of the Tango and Mango spacecraft are used to compute the a-priori relative dynamics state vector $\Delta\hat{\mathbf{x}}^-$, which in turn is projected to the $\mathcal{H}$ frame. Consequently, the a-priori filter state vector can be formed by including the propagated biases (according to equation (6)), as $\hat{\mathbf{y}}^-(t_e) = [\Delta\hat{\mathbf{x}}^-(t_e), \mathbf{b}^-(t_e)]^T$.

To complete the time update of the filter algorithm, it is necessary to propagate the error covariance matrix $\mathbf{P}$, associated with the estimated state. Assuming that a matrix $\mathbf{P}^+(t_0)$ is available, the uncertainty of the state can be propagated by using a linearised dynamical model based on a given STM, as shown in Table 1. Considering a bias propagation matrix $\mathbf{G}(t_e, t_0) = \mathbf{1}_{3\mathrm{x}3}$, the matrix $\mathbf{P}^+(t_0)$ can be propagated to time t_e using the augmented STM $\mathbf{\Phi}$ given by equation (7), by means of the Lyapunov equation, as follows

$$\mathbf{P}^-(t_e) = \mathbf{\Phi}(t_e, t_0)\mathbf{P}^+(t_0)\mathbf{\Phi}^T(t_e, t_0) + \mathbf{Q} \tag{10}$$

Once the time update provides the a-priori value for the state vector $\hat{\mathbf{y}}^-(t_e)$ and its associated covariance matrix $\mathbf{P}^-(t_e)$, the filter innovation can be computed. At this point, the filter distinguishes between LOS measurements and GPS measurements, namely the execution time $t_e = t_L || t_G$. When computing the innovation due to LOS measurements (i.e. $t_e = t_L$), distance measurements are included in the algorithm by computing an estimate of the relative distance between both spacecraft at time $t_d = t_L - \delta t$, where δt is the delay between both types of measurements. Following (Delpech, et.al., 2009), the estimated distance at time t_d

can be computed by using the measurement model h^d given by equation (4a), the distance rate $\dot{d}$ and the external acceleration a_e projected along the distance vector, as follows

$$\hat{d} = h^d(\hat{\mathbf{y}}^-(t_L)) - \dot{d}(t_L)\delta t - \frac{1}{2}a_e(t_L, \delta t)\delta t^2 \tag{11}$$

The innovation due to distance requires the linearised model $\mathbf{H}^d$, the distance measurement vector $\mathbf{z}^d(t_d)$, (formed out of the distance measurement in equation (3)) and the estimated distance $\hat{d}(t_d)$. Additionally, given that the measurement correction is given at time t_d, this correction must be propagated to time t_d so that it can be applied to the innovation equation. Thus, the complete measurement update can be computed as follows

$$\mathbf{K}^d(t_L) = \mathbf{P}^-(t_L)(\mathbf{H}^d(t_L))^T(\mathbf{H}^d(t_L)\mathbf{P}^-(t_L)(\mathbf{H}^d(t_L))^T + \mathbf{R}^d)^{-1} \tag{12a}$$

$$\hat{\mathbf{y}}^{d+}(t_L) = \hat{\mathbf{y}}^-(t_L) + \mathbf{\Phi}(t_L, t_d)\mathbf{K}^d(t_L)[\mathbf{z}^d(t_d) - \hat{d}(t_d)] \tag{12b}$$

$$\mathbf{P}^{d+}(t_L) = \mathbf{P}^-(t_L) - \mathbf{K}^d(t_L)\mathbf{H}^d(t_L)\mathbf{P}^-(t_L) \tag{12c}$$

The measurement update due to LOS measurements is now computed by using the current best estimate $\hat{\mathbf{y}}^{d+}$ and corresponding error covariance matrix $\mathbf{P}^{d+}$. In addition, this innovation uses the measurement model h^l, its linearised version $\mathbf{H}^l$ and the LOS measurement vector $\mathbf{z}^l(t_L)$ (formed out of LOS measurements in equation (3)), as follows

$$\mathbf{K}^l(t_L) = \mathbf{P}^{d+}(t_L)(\mathbf{H}^l(t_L))^T(\mathbf{H}^l(t_L)\mathbf{P}^{d+}(t_L)(\mathbf{H}^l(t_L))^T + \mathbf{R}^l)^{-1} \tag{13a}$$

$$\hat{\mathbf{y}}^+(t_L) = \hat{\mathbf{y}}^{d+}(t_L) + \mathbf{K}^l(t_L)[\mathbf{z}^l(t_L) - h^l(\hat{\mathbf{y}}^{d+}(t_L))] \tag{13b}$$

$$\mathbf{P}^+(t_L) = \mathbf{P}^{d+}(t_L) - \mathbf{K}^l(t_L)\mathbf{H}^l(t_L)\mathbf{P}^{d+}(t_L) \tag{13c}$$

For the case of GPS measurements, an analogous procedure can be followed. Given a measurement availability rate of 0.1 Hz (0.05 Hz in some phases), a complete state update is performed exactly when a GPS measurement is available. Following a time update given by equations (9)-(10) at time $t_e = t_G$, the innovation due to GPS is computed by using the measurement model h^g, its linearised version $\mathbf{H}^g$ and the GPS measurement vector $\mathbf{z}^g(t_G)$ (as given by equation (1)), as follows

$$\mathbf{K}^g(t_G) = \mathbf{P}^-(t_G)(\mathbf{H}^g(t_G))^T(\mathbf{H}^g(t_G)\mathbf{P}^-(t_G)(\mathbf{H}^g(t_G))^T + \mathbf{R}^g)^{-1} \tag{14a}$$

$$\hat{\mathbf{y}}^+(t_G) = \hat{\mathbf{y}}^-(t_G) + \mathbf{K}^g(t_G)[\mathbf{z}^g(t_G) - h^g(\hat{\mathbf{y}}^-(t_G))] \tag{14b}$$

$$\mathbf{P}^+(t_G) = \mathbf{P}^-(t_G) - \mathbf{K}^g(t_G)\mathbf{H}^g(t_G)\mathbf{P}^-(t_G) \tag{14c}$$

From the estimated vector $\hat{\mathbf{y}}^+(t_e)$ resulting from filter innovation due to FFRF LOS or GPS measurements, it is possible to extract the estimated relative state vector $\Delta\hat{\mathbf{x}}^+(t_e)$ and rotate it to the $\mathcal{I}$ frame so that the absolute orbits of both spacecraft can be retrieved for the next time update.

3.3.3 Manoeuvre handling

Several possible approaches have been discussed recently to handle the presence of manoeuvres in tracking problems (D'Amico, et.al., 2009). The heuristic approach used in the present study assumes some degree of knowledge of the applied manoeuvres on the Mango spacecraft (obtained from off-line processing) but considers also an increment on the state covariance matrix at specific epochs, namely the uncertainty of the manoeuvring activity is considered to be spanned over the total manoeuvre burn. In this way, given the a-priori knowledge of an applied thrust, it is discretized according to its duration and timing in order to apply specific control inputs at every execution t_e (according to equation (8a)) by forming the input vector $\mathbf{u}$ from the available information. Similarly, the process noise covariance matrix $\mathbf{Q}$ in equation (10) is incremented into matrix $\mathbf{Q}_c$ at every time update under the presence of manoeuvres, considering the uncertainty in the manoeuvring activities given by matrix $\mathbf{Q}_m$. Thus,

$$\mathbf{Q}_c = \mathbf{Q} + \mathbf{Q}_m \tag{15}$$

where the general structure of matrix $\mathbf{Q}_m$ implies the inclusion of error covariance terms in the relative velocity expressed in the $\mathcal{H}$ frame.

Additionally, the manoeuvre activities affect LOS measurements due to the increment of multipath effects. These effects are present during the execution of a special attitude guidance mode and this period may reach few minutes. Hence, the LOS measurement noise covariance matrix $\mathbf{R}^l$ must be adapted during those epochs, considering a maximum bias offset of 2^{o}, so that the measurement weight in the innovation step is reduced when the multipath is likely (Delpech, et.al., 2011; Guidotti, et.al., 2011).

4 Validation of results

The filter design developed in the present study has been tested using FFRF and GPS flight data obtained from the PRISMA nominal phase. For this purpose, the filter has been tuned up targeting to the best performance by selecting specific values for the process noise covariance matrix and by setting the proper measurement noise covariance matrices.

For simplicity, the process noise covariance matrix $\mathbf{Q}$ is assumed to have a diagonal form with sub-matrices $q_{\Delta \mathrm{r}}$, $q_{\Delta \dot{\mathrm{r}}}$ and q_b for relative position, relative velocity and FFRF float biases, respectively. The chosen standard deviations for such sub-matrices after the tuning process are shown in Table 2. The higher process noise assigned to the YLOS bias propagation has been chosen so that the filter relies more on measurements, allowing in this way to better follow the YLOS bias fluctuations. In addition, these quantities are specified for the case of a J2 gravity model. If instead a linear model for state propagation is used, higher values for $q_{\Delta \mathrm{r}}$ and $q_{\Delta \dot{\mathrm{r}}}$ could be selected in order to compensate for additional process noise induced by linearisation.

The measurement noise covariance matrices $\mathbf{R}^l$, $\mathbf{R}^d$ and $\mathbf{R}^g$ for FFRF LOS, FFRF distance and GPS observables, respectively, are tuned up by taking the noise statistics of the measurements and are also considered to have a diagonal form (indicating uncorrelated measurements). The chosen standard deviations are also shown in Table 2. The values assigned to matrices $\mathbf{Q}$ and $\mathbf{R}$ reflect a higher dependence of the filter on the relative dynamics model given the kinematic nature of the FFRF and GPS measurements.

Table 2 Tuning values for relative navigation filter

Matrix	Component	Std
$\mathbf{Q}$	$q_{\Delta \mathbf{r}}$	$1 \cdot 10^{-5}$ m
	$q_{\Delta \dot{\mathbf{r}}}$	$1 \cdot 10^{-6}$ m/s
		$7.5 \cdot 10^{-5}$ deg
	q_b	$2.3 \cdot 10^{-4}$ deg
		$1 \cdot 10^{-5}$ m
$\mathbf{R}^d$		0.04 m
$\mathbf{R}^l$		0.16 deg
		0.21 deg
$\mathbf{R}^g$		0.015 m
		0.006 m
		0.007 m

The filter starts at epoch 2010/10/28:16:30:00 UTC by computing a rough initial state obtained from the available FFRF and GPS measurements. It is first executed during an initial data arc of 8 hours (during which the formation has an inter-spacecraft distance of around 300 m on average) using either single-sensor or sensor fusion modes in order to evaluate the achieved accuracy. The results are presented in Table 3. The main purpose of this assessment is to ensure the overall preservation of the resulting accuracy, regardless of the sensor(s) being used. This condition represents the premise for the evaluation of the filter performance on larger data sets.

Table 3 Consistency of filtered relative navigation and POD at a separation of ≈300 m

Sensor	Error in position (cm)			Error in velocity (mm/s)		
	Radial	Along-track	Cross-track	Radial	Along-track	Cross-track
FFRF	0.1 ± 2.7	-0.3 ± 2.3	1.4 ± 12.6	-0.01 ± 0.10	0.00 ± 0.04	0.06 ± 0.15
GPS	0.2 ± 1.6	0.1 ± 0.6	0.3 ± 0.8	0.01 ± 0.22	0.00 ± 0.07	0.00 ± 0.21
FFRF+GPS	0.3 ± 1.5	0.1 ± 1.0	0.3 ± 0.6	0.00 ± 0.09	0.00 ± 0.04	0.00 ± 0.07

As observed in Table 3, the general accuracy obtained from single-sensor modes is fairly similar, which provides an indication of the effective use of dynamical filtering on FFRF measurements, considering the quality of GPS measurements (see Figure 3). As indicated in previous analyses (Delpech, et.al., 2009, 2011; Guidotti, et.al., 2011), a solution with lower precision in the cross-track component can be expected when only FFRF measurements are used. This is caused by the high sensitivity of this component to FFRF LOS measurement inaccuracies (multipath and other bias errors, as seen in Figure 4) due to its dynamical uncoupling from the in-plane components. In addition, the final errors resulting from unfixed angular measurements during dynamical filtering are distance dependent. On the other hand, as indicated in Table 3, the overall accuracy obtained from the filter using measurements from both sensors is preserved or slightly improved.

Once the general preservation of accuracy is ensured, the filter is executed again with the capability of using measurements from both sensors, during a 50-hours data arc in order

Figure 5 Filtered in-plane relative position showing the formation flying operations (indicated in figure) from 2010/10/28-16:30 to 2010/10/30-18:30 UTC. The trajectory of the Mango spacecraft starts at the left hand side with a stand-by operation at approx. 300 m of relative distance in the along-track direction.

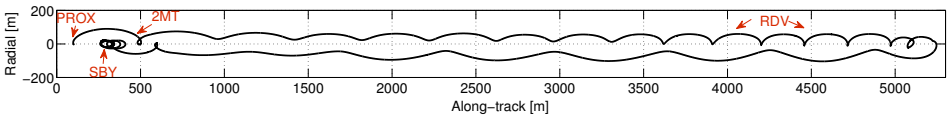

to further analyse other characteristics. With the purpose of introducing the analysis of the delivered solution, Figure 5 depicts the filtered in-plane relative position showing some representative formation flying operations executed during this mission phase, including a rendezvous manoeuvre during which the Mango spacecraft is taken to a relative distance of more than 5 km in the along-track component

One of the main drivers of the filter design presented in this study is the increment of availability, reliability and robustness of the provided relative navigation solution. Typical single-sensor or isolated-sensor systems may be prone to errors or limited operation periods due to different sensor availability phases caused by an unexpected failure or mission orbit design. To this end, one particular feature of the filter is the capability of not only using FFRF and GPS measurements at the same time, but also managing data outages from a given sensor by providing relative navigation solutions using measurements from the available sensor. In order to test these filter properties, some artificial outages have been introduced to the FFRF and GPS data arcs so as to depict different conditions of sensor availability. For the case of the FFRF sensor a data gap might occur due to low quality or invalid measurements as declared by the instrument. On the other hand, a data gap from GPS sensor failure is certainly more unlikely due to the possibility of implementation of cold redundancy, as in the case of PRISMA (Ardaens, et.al., 2012; D'Amico, et.al., 2009). Instead, GPS data outages might happen during a mission in a HEO where the formation experiences orbit phases with poor GPS coverage.

To analyse the performance of the relative navigation filter, two (artificial) FFRF data gaps have been introduced. The first one with duration of 2 hours starts at epoch 2010/10/28-20:00:00 UTC whereas the second one is 1-hour long and starts at epoch 2010/10/29-12:42:00 UTC. Likewise, two (artificial) GPS data gaps with duration of 11.7 hours each have been introduced considering the signal availability that the formation would experience in HEO with a typical orbital period of 19.7 hours. The filter accuracy is assessed by using POD products and the errors in the filtered relative position are shown in Figure 6.

The filter starts using measurements from both FFRF and GPS sensors. Given the accuracy of the data provided by the two instruments and the formation state during the initialization period (see Figure 6), the filter converges quickly. The first FFRF data gap is coped by the filter through the execution of a handover to the use of solely GPS measurements. The state error during a transition between sensors is properly managed by considering different observation and measurement models, as given by equations (1)-(4). Although dynamic propagation could be used during this data outage, the relative dynamics of the formation is hardly known to a level that matches the accuracy of measurements and a degraded solution would be expected. This condition may become critical if the two spacecraft are executing formation flying operations, such as those depicted in Figure 5.

Figure 6 Consistency of the filtered relative position and POD using measurements from FFRF and GPS sensors from 2010/10/28-16:30 to 2010/10/30-18:30 UTC. Individual sets of letters indicate sensor use. F denotes FFRF, G denotes GPS whereas FG denotes FFRF plus GPS.

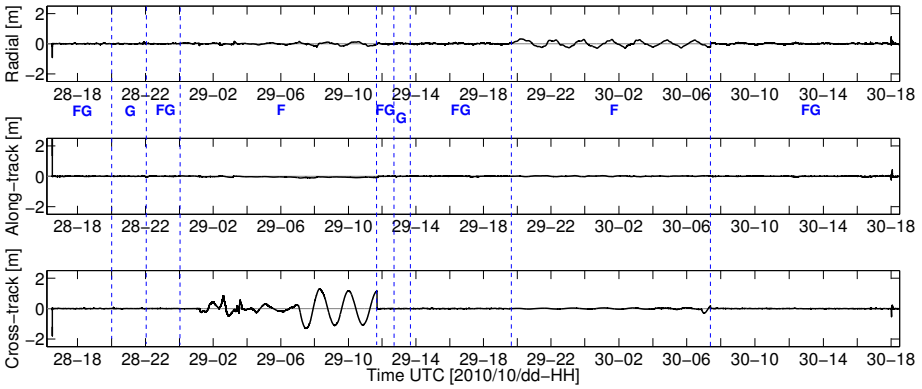

Once the accuracy of the FFRF measurements is restored, the filter uses again redundant observations from both sensors at epoch 2010/10/28-22:00:00 UTC. During this phase the filter ensures redundancy of observations, thus providing a more reliable solution. Due to the presence of a GPS data outage starting at epoch 2010/10/29-00:00:00 UTC, the filter performs a handover to the use of solely FFRF measurements. In this way, the availability of the solution with similar levels of accuracy is guaranteed from a single relative navigation filter. However, large errors are expected especially in the cross-track component due to the increasing relative distance during this orbit phase. The use of GPS measurements starting from epoch 2010/10/29-11:42:00 UTC provides an aid to fix some errors caused by the large relative distance in the FFRF measurements, for which the filter cannot provide the corrections at the required level. In particular, the GPS measurements help to correct some errors in YLOS bias estimation. This is translated to an improvement in the precision of the solution in the cross-track component even after a handover to the use of only FFRF measurements is executed at epoch 2010/10/29-19:42:00 UTC, while the Mango spacecraft is performing a rendezvous manoeuvre.

During the last phase of the data arc under analysis, the filter completes one more handover procedure. The GPS data availability period is extended and the filter uses measurements from both sensors during this period when the Mango spacecraft executes a 2-Manoeuvre Transfer and a Proximity operation (see Figure 5). During this intense manoeuvring period, the FFRF measurements are highly affected by multipath, as shown in Figure 4. The redundancy of observations through the use of GPS data during this phase makes the solution less prone to errors. The use of the sensor fusion concept is especially appealing during this period, given that the provided solution is not only more reliable but also more robust.

5 Conclusion

The design and implementation of a simple, yet accurate, relative navigation filter using measurements from the FFRF and GPS sensors has been presented. It makes use of simple

relative dynamics models and numerical integration methods in order to demonstrate the feasibility of using measurements from different RF metrology systems so as to provide a single relative navigation solution. The filter has been tested using flight data from both sensors during the PRISMA mission nominal phase. Setting the similar accuracy achieved by single-sensor solutions as a premise, the performance of the filter has been analysed in the presence of different sensor availability stages, which might result from unexpected failures or mission orbit design. The use of measurements from both sensors at the same orbit phases provides robustness to the solution (through redundancy of observations), making it less prone to errors due to bad data points. In addition, by having the capability of performing handover operations between sensors, the relative navigation filter guarantees a single solution with similar levels of accuracy and increased availability.

Due to its simplicity, the accuracy of the present design is limited to the use of measurements. In order to further increase the availability of acceptable solutions when no measurements are present, both an enhanced dynamical model and numerical integration method would be required. Additionally, although the GPS measurements used in the present study were generated off-line, future research in PPP techniques for navigation in LEO might provide measurements with similar quality, enabling the possibility of real-time relative navigation using measurements from FFRF and GPS sensors.

Note

This paper is a revised and expanded version of a paper entitled 'Radio-frequency sensor fusion for relative navigation of formation flying satellites' presented at the 5th International Conference on Spacecraft Formation Flying Missions and Technologies (SFFMT), Munich, Germany, 29-31 May 2013.

References

D'Errico, M. (Ed.) (2013), 'Distributed Space Missions for Earth System Monitoring', Springer.

Pinard, D., Reynaud, S., Delpy, P., Strandmoe, S.E. (2007) 'Accurate and Autonomous Navigation for the ATV', *Aerospace Science and Technology*, Vol. 11, pp. 490–498.

Jäggi, A., Hugentobler, U., Bock, H., Beutler, G. (2007) 'Precise Orbit Determination for GRACE using Undifferenced or Double Differenced GPS Data', *Advances in Space Research*, Vol. 39, pp. 1612–1619.

Montenbruck, O., Wermuth, M., Kahle, R. (2011) 'GPS Based Relative Navigation for the TanDEM-X Mission - First Flight Results', *NAVIGATION, Journal of the Institute of Navigation*, Vol. 58, No. 4, pp. 293–304.

Grelier, T., Guidotti, P.Y., Delpech M., Harr, J., Thevenet, J.B., Leyre, X. (2010) 'Formation Flying Radio Frequency Instrument: First Flight Results from the PRISMA Mission'. Paper Presented at the *5th ESA Workshop on Satellite Navigation Technologies*. 8-10 December 2010. Noordwijk, Netherlands.

Kroes, R. (2006) 'Precise Relative Positioning of Formation Flying Spacecraft using GPS'. PhD Thesis, TU Delft.

Delpech, M., Guidotti, P.Y., Djalal, S., Grelier, T., Harr, J. (2009) 'RF Based Navigation for PRISMA and other Formation Flying Missions in Earth Orbit'. Paper Presented at the *21st International Symposium on Space Flight Dynamics*. 28 September-2 October 2009. Toulousse, France.

Ardaens, J.-S., D'Amico, S., Cropp, A. (2013) 'GPS-Based Relative Navigation for the PROBA-3 Formation Flying Mission', *Acta Astronautica*, Vol. 91, pp. 341–355.

D'Amico, S., Ardaens, J.-S., Montenbruck O. (2009) 'Navigation of Formation Flying Spacecraft using GPS: the PRISMA Technology Demonstration'. Paper Presented at the *ION-GNSS-2009 Conference*. 22-25 September 2009. Savannah, USA.

D'Amico, S., Ardaens, J.-S., Larsson, R. (2012) 'Spaceborne Autonomous Formation Flying Experiment on the PRISMA Mission', *Journal of Guidance, Control and Dynamics*, Vol. 35, No. 3, pp. 834–850.

Ardaens, J.-S., D'Amico, S., Montenbruck, O. (2012) 'Final Commissioning of the PRISMA GPS Navigation System', *Journal of Aerospace Engineering, Sciences and Applications*, Vol. 4, No. 3, pp. 104–118.

Hauschild, A., Montenbruck, O. (2008) 'Real-time Clock Estimation for Precise Orbit Determination of LEO-Satellites'. *Proceedings of the 21st International Technical Meeting of the Satellite Division of The Institute of Navigation (ION GNSS 2008)*. September 16-19 2008. Savannah, USA.

Hall, D., Llinas, J. (1997) 'An Introduction to Multisensor Data Fusion', *Proceedings of the IEEE*, Vol. 85, pp. 6–23.

Durrant-Whyte, H. (2001) *Multi Sensor Data Fusion*. http://www.acfr.usyd.edu.au/pdfs/training/multiSensorDataFusion/dataFusionNotes.pdf (Accessed Feb 2015).

Liggins, M., Hall, D., Llinas, J. (Eds.) (2008), 'Handbook of Multisensor Data Fusion: Theory and Practice', CRC Press.

Delpech, M., Guidotti, P.Y., Grelier, T., Seguela, D., Berges, J.C., Djalal, S., Harr, J. (2011) 'First Formation Flying Experiment Based on a Radio Frequency Sensor: Lessons Learned and Perspectives for Future Missions'. Paper Presented at the *4th International Conference on Spacecraft Formation Flying Missions and Technology*. May 18-20 2011. Quebec, Canada.

Guidotti, P.Y., Delpech, M., Berges, J.C., Djalal, S., Grelier, T., Seguela, D., Harr, J. (2011) 'Flight Results of the FFIORD Formation Flying Experiment'. Paper Presented at the *4th International Conference on Spacecraft Formation Flying Missions and Technology*. May 18-20 2011. Quebec, Canada.

Clohessy, W. H., Wiltshire, R. S. (1960) 'Terminal Guidance for Satellite Rendezvous', *Journal of Aerospace Sciences*, Vol. 27, pp. 653–658.

Hill, G.W. (1878) 'Researches in the Lunar Theory', *American Journal of Mathematics*, Vol. 1, No. 1, pp. 5–26.

Alfriend, K.T., Vadali, S.R., Gurfil, P., How, J.P., Breger, L.S. (2010), 'Spacecraft Formation Flying: Dynamics, Control and Navigation', Elsevier Ltd.

Yamanaka, K., Ankersen, F. (2002) 'New State Transition Matrix for Relative Motion on an Arbitrary Elliptical Orbit', *Journal of Guidance, Control and Dynamics*, Vol. 25, pp. 60–66.

Gim, D.W., Alfriend, K.T. (2003) 'State Transition Matrix of Relative Motion for the Perturbed Noncircular Reference Orbit', *Journal of Guidance, Control and Dynamics*, Vol. 26, No.6, pp. 956–971.

Montenbruck, O., Kirschner, M., D'Amico, S., Bettadpur, S. (2006) 'E/I-Vector Separation for Safe Switching of the GRACE Formation', *Aerospace Science and Technology*, Vol. 10, pp. 628–635.

D'Amico, S., Montenbruck, O. (2006) 'Proximity Operations of Formation Flying Spacecraft using Eccentricity/Inclination Vector Separation', *AAIA Journal of Guidance, Control and Dynamics*, Vol. 29, No. 3, pp. 554–563.